Elliptical dichroism in biharmonic ionization of atoms

J. Hofbrucker [1,2] B. Böning [1,2] A. V. Volotka [3] and S. Fritzsche [1,2,4]

[1]*Helmholtz-Institut Jena, Fröbelstieg 3, D-07743 Jena, Germany*

[2]*GSI Helmholtzzentrum für Schwerionenforschung GmbH, Planckstrasse 1, D-64291 Darmstadt, Germany*

[3]*Department of Physics and Engineering, ITMO University, Kronverkskiy prospekt 49, 197101 St. Petersburg, Russia*

[4]*Theoretisch-Physikalisches Institut, Friedrich-Schiller-Universität Jena, Max-Wien-Platz 1, D-07743 Jena, Germany*

(Received 25 March 2021; accepted 17 June 2021; published 1 July 2021)

In multiphoton ionization of atoms, elliptical dichroism may arise in the photoelectron angular distributions due to the interference of the possible ionization pathways. We here consider the interaction of atoms with an elliptically polarized biharmonic ($\omega + 2\omega$) field which simultaneously allows one- and two-photon ionization of the atoms. The interference between these two ionization pathways introduces contributions to the elliptical dichroism in addition to the dichroism that arises from the two-photon ionization alone. We show that these additional dichroism contributions can lead to a stronger dichroism in comparison to the one arising from two-photon ionization only. We present a relativistic analysis of the corresponding photoelectron angular distributions and discuss individual contributions to the dichroic phenomena. Detailed computations have been performed for biharmonic ionization of neutral helium atoms.

DOI: 10.1103/PhysRevA.104.013102

I. INTRODUCTION

Biharmonic ionization of atoms is often used to refer to the photoionization by light beams that consist of two co-propagating components with frequencies which are integer multiples of some fundamental frequency ω, i.e., $n\omega + m\omega$. In biharmonic ionization, therefore, $n\omega$ and $m\omega$ multiphoton ionization may both result in the same final state of the photoelectron (and ion). The photoelectron wave function is then composed of the contributions of both ionization paths as well as their *interference*.

Biharmonic ionization has been extensively studied at low frequencies in the so-called strong-field regime, especially for the ionization of atoms by counter-rotating circularly polarized light, which, similarly, is often referred to as bicircular ionization [1–6]. In the strong field regime, the interaction of atoms with biharmonic fields was utilized to control the ionization process by changing the polarization properties as well as energy of the beams. For example, biharmonic ionization can be used to create and control electron vortices [7–9], to generate circularly polarized high-order harmonic fields [10] and high-order harmonic beams with well-defined orbital angular momentum [11], or to carry our phase-of-the-phase spectroscopy measurements [12].

Biharmonic beams at XUV photon energies can nowadays be generated by free-electron lasers due to the (coherent) superposition of the beams generated at such facilities. The first pioneering experiments were carried out for the ionization of helium and neon by linearly polarized biharmonic beams and showed that this process can be used to characterize the phase and amplitude of the biharmonic light beam [13–15]. While the majority of free-electron lasers presently provide linearly polarized beams, several facilities already allow control of the polarization or will make this possible in planned future upgrades [16,17]. The experimental possibilities of the production of biharmonic beams at XUV energies also sparked theoretical efforts. In particular, the photoelectron angular distributions of biharmonic ionization with linearly and circularly polarized beams which comprise a fundamental frequency and its second harmonic ($\omega + 2\omega$) were studied extensively [18–20] including the influence of ultrashort pulse length in the ionization process [21]. Recently, it was shown that the photoelectron angular distribution can be experimentally controlled by the intensities and phase of two circularly polarized beam components in biharmonic ionization of arbitrary order (i.e., $n\omega + m\omega$) [22].

Another interesting phenomenon occurs in the interaction of atoms with elliptically polarized light. In contrast to pure circular photon polarization states, the interaction of unpolarized atoms with elliptically polarized light gives rise to dichroic phenomena. Already in multiphoton ionization of atoms by monochromatic light, the sensitivity to light handedness can be observed in the photoelectron angular distributions [23–29]. The dependence of these distributions on the handedness of the ionizing light is called *elliptical dichroism*, and its origin as well as maximum were described in detail for two-photon ionization of neutral atoms [30]. While in monochromatic ionization of s electrons by elliptically polarized light the dichroism arises from a single contribution (within electric dipole approximation) to the photoelectron angular distributions, in biharmonic ionization (e.g., $\omega + 2\omega$) the dichroism becomes (much) more complex. In addition to the contribution arising from the two-photon ionization, the interference between the one- and two-photon ionization introduces additional contributions to the dichroism. The aim of this paper is to analyze and characterize these contributions

and show that they can enhance the elliptical dichroism in comparison to the pure two-photon ionization process.

The paper is organized as follows. In Sec. II, we provide a relativistic description of biharmonic ionization within second-order perturbation theory. To disentangle the contributions to the elliptical dichroism clearly, we reduce the theoretical approach to the nonrelativistic limit. Section III presents our main results and demonstrates the dependency of elliptical dichroism in photoelectron angular distributions on the beam parameters such as the energy as well as the intensities of the beam components. Finally, a summary of this paper with an outlook on further progress is provided in Sec. IV. Relativistic units ($\hbar = c = m = 1$) are used throughout the paper unless otherwise stated.

II. THEORY

A. General theory

The vector potential of a biharmonic beam consisting of two components with a fundamental frequency ω and its second harmonic copropagating along the quantization axis $\hat{\boldsymbol{k}}||\hat{z}$ can be written as

$$\boldsymbol{A}(\boldsymbol{r},t) = A_0^{(\omega)}\boldsymbol{A}^{(\omega)}(\boldsymbol{r},t) + e^{i\Phi}A_0^{(2\omega)}\boldsymbol{A}^{(2\omega)}(\boldsymbol{r},t), \tag{1}$$

where each individual vector potential takes the form

$$\boldsymbol{A}^{(n\omega)}(\boldsymbol{r},t) = \boldsymbol{\varepsilon}^{(n\omega)}e^{-in\omega t + i\boldsymbol{k}^{(n\omega)}\boldsymbol{r}}, \tag{2}$$

where $A_0^{(n\omega)}$ is the amplitude of the vector potential of each component that is directly proportional to the flux of the component $F^{(n\omega)} = (A_0^{(n\omega)})^2$ and to the intensity $I^{(n\omega)} = n\omega F^{(n\omega)}$. The phase shift between the two beam components is given by Φ. The polarization of each component is denoted by $\boldsymbol{\varepsilon}^{(n\omega)}$, which can be expressed in terms of the ellipticity $\gamma^{(n\omega)}$ and the basis vectors in helicity representation $\boldsymbol{\varepsilon}_{\pm1}$ as

$$\boldsymbol{\varepsilon}^{(n\omega)} = \frac{\boldsymbol{\varepsilon}_{-1}[1-\gamma^{(n\omega)}] - \boldsymbol{\varepsilon}_{+1}[1+\gamma^{(n\omega)}]}{\sqrt{2[1+(\gamma^{(n\omega)})^2]}}. \tag{3}$$

The ellipticity can take values in the range $-1 \leqslant \gamma^{(n\omega)} \leqslant 1$, where $\gamma^{(n\omega)} = -1$ corresponds to left-circularly, $\gamma^{(n\omega)} = 0$ to linearly, and $\gamma^{(n\omega)} = 1$ to right-circularly polarized light. The interaction of the biharmonic field composed of a fundamental frequency and its second harmonic (1) with an atom in an initial many-electron state $|\alpha_i J_i M_i\rangle$ can lead to the ionization of the atom by absorption of one photon with energy 2ω or two photons with energy ω; see Fig. 1. After the interaction, the system (ion + photoelectron) is left in a final state $|\alpha_f J_f M_f, \boldsymbol{p}_e m_e\rangle$. The atomic states are described by the total angular momentum J, its projection M, and further quantum numbers α which are necessary to uniquely describe the atomic state. The photoelectron wave function is characterized by its momentum $\boldsymbol{p}_e$ and spin projection m_e. The ionization proceeds via one- and two-photon ionization into a final state with identical energy. It has been shown before that the ionization of atoms by long pulses, as they are often produced by the current free-electron laser facilities, can be well described with the assumption of infinitely long pulses [15,31,32]. Since we focus on ionization at such facilities, we will adopt the long pulse approximation. The one- and two-photon ionization processes can then be described within lowest order perturbation theory by the transition amplitudes

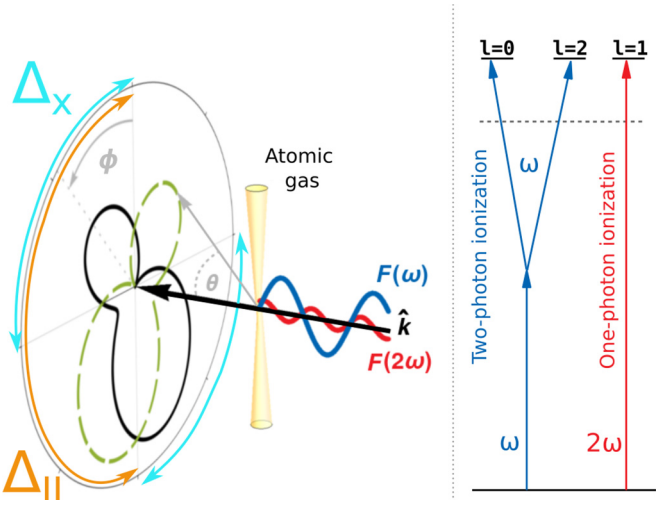

FIG. 1. Schematic representation of biharmonic ionization of atoms by elliptically polarized light. Energy scheme diagram of $\omega + 2\omega$ biharmonic ionization (right). The biharmonic beam is composed of two co- or counter-rotating components with energy ω as well as its second-order harmonic with energy 2ω and their corresponding fluxes $F^{(\omega)}$ and $F^{(2\omega)}$. The photoelectron angular distributions of ionization of atoms by such a biharmonic field are detected in the polarization plane ($\theta = \pi/2$) as functions of the azimuthal angle ϕ. The azimuthal angle is measured from the linear part of the polarization vector, which coincides for both beam components. Two example distributions are shown and correspond to the ionization of atoms by beams of opposite handedness. Their difference is used to define the elliptical dichroism in the polarization plane. To disentangle the two fundamental contributions to the elliptical dichroism, two dichroism parameters are defined, $\Delta_{||}$ and $\Delta_\times$. While the dichroism $\Delta_{||}$ is defined as a difference of ionization rates integrated over the left semiplane, i.e., $0 \leqslant \phi \leqslant \pi$ (orange arrow), $\Delta_\times$ is defined using the sum of integrals $0 \leqslant \phi \leqslant \pi/2$ and $\pi \leqslant \phi \leqslant 3\pi/2$ (turquoise arrows).

$$M^{(2\omega)}_{M_i M_f m_e} = \langle \alpha_f J_f M_f, \boldsymbol{p}_e m_e | \boldsymbol{\alpha}\cdot\boldsymbol{A}^{(2\omega)} | \alpha_i J_i M_i\rangle, \tag{4}$$

$$M^{(\omega)}_{M_i M_f m_e} = \sum_\nu \langle \alpha_f J_f M_f, \boldsymbol{p}_e m_e | \boldsymbol{\alpha}\cdot\boldsymbol{A}^{(\omega)} | \alpha_\nu J_\nu M_\nu\rangle \times \frac{\langle \alpha_\nu J_\nu M_\nu | \boldsymbol{\alpha}\cdot\boldsymbol{A}^{(\omega)} | \alpha_i J_i M_i\rangle}{E_i + \omega - E_\nu}, \tag{5}$$

respectively, with $\boldsymbol{\alpha}$ being the vector of Dirac matrices and $\boldsymbol{A}^{(n\omega)}$ being the photon fields. We here employ the independent particle approximation, where the electron wave function is represented by a single active electron, while all other electrons are accounted for by a screening potential in the Hamiltonian of the Dirac equation. Due to the interaction of the atom with the electromagnetic field, the active electron from the substate described by the principal n_a, relativistic κ_a, quantum numbers as well as projection of the total angular momentum m_a given by $|a\rangle \equiv |n_a \kappa_a m_a\rangle$ of the atom is promoted into the continuum, leaving a vacancy in the atomic substate. The relativistic quantum number κ_a is related to the total (j_a) and orbital (l_a) angular momentum

quantum numbers as $\kappa = (-1)^{l_a+j_a+1/2}(j_a+1/2)$. In the second quantization formalism, the final many-electron state can be described by a Slater determinant wave function with the use of the electron creation $a^\dagger_{\boldsymbol{p}_e m_e}$ and annihilation operators $a_{n_a\kappa_a m_a}$ and the Clebsch-Gordan coefficients $\langle .., .|. \rangle ..$ as

$$|\alpha_f J_f M_f, \boldsymbol{p}_e m_e\rangle = \sum_{m_a M} \langle j_a - m_a, J_i M | J_f M_f\rangle \times (-1)^{j_a-m_a} a^\dagger_{\boldsymbol{p}_e m_e} a_{n_a\kappa_a m_a} |\alpha_i J_i M\rangle. \quad (6)$$

Together with the independent particle approximation, the above expression allows us to reduce the many-electron amplitudes (4) and (5) to amplitudes which depend only on one-electron wave functions of the active electron,

$$M^{(2\omega)}_{M_i M_f m_e} = \sum_{m_a} \langle j_a - m_a, J_i M_i | J_f M_f\rangle (-1)^{j_a-m_a} \times \langle \boldsymbol{p}_e m_e | \boldsymbol{\alpha}\cdot\boldsymbol{A}^{(2\omega)} | a\rangle, \quad (7)$$

and

$$M^{(\omega)}_{M_i M_f m_e} = \sum_{m_a} \langle j_a - m_a, J_i M_i | J_f M_f\rangle (-1)^{j_a-m_a} \times \sum_n \frac{\langle \boldsymbol{p}_e m_e | \boldsymbol{\alpha}\cdot\boldsymbol{A}^{(\omega)} | n\rangle \langle n | \boldsymbol{\alpha}\cdot\boldsymbol{A}^{(\omega)} | a\rangle}{E_a + \omega - E_n}, \quad (8)$$

where a summation over the complete energy spectrum of single-electron intermediate states $|n\rangle$ is to be carried out. To evaluate the transition amplitudes numerically, it is convenient to carry out further expansions. First, the electromagnetic field $\boldsymbol{A}^{(n\omega)}$ can be decomposed into spherical tensors with electric ($p=1$) and magnetic ($p=0$) components with multipolarity J using

$$\boldsymbol{A}^{(n\omega)} = 4\pi \sum_{JMp} i^{J-p} \left[\boldsymbol{\varepsilon}^{(n\omega)} \cdot \boldsymbol{Y}^{(p)*}_{JM}(\hat{\boldsymbol{k}})\right] \boldsymbol{a}^{(p)}_{JM}(\boldsymbol{r}). \quad (9)$$

Additionally, we also expand the photoelectron wave function in the spherical basis into its partial wave components

$$|\boldsymbol{p}_e m_e\rangle = \frac{1}{\sqrt{E_e|\boldsymbol{p}_e|}} \sum_{jm_j}\sum_{lm_l} i^l e^{-i\delta_\kappa} \langle l m_l, 1/2 m_e | j m_j\rangle \times |E_e \kappa m_j\rangle Y^*_{lm_l}(\theta,\phi), \quad (10)$$

where the electron energy is given by $E_e = \sqrt{\boldsymbol{p}_e^2 + 1}$, the phases of partial waves by δ_κ, and the emission direction of the photoelectron in terms of polar and azimuthal angles θ and ϕ by the spherical harmonics $Y_{lm_l}(\theta,\phi)$ (see Fig. 1). We can use these expansions to analyze the one- and two-photon ionization amplitudes $M^{(2\omega)}_{M_i M_f m_e}$ and $M^{(\omega)}_{M_i M_f m_e}$ and to derive the associated observables. The explicit forms of the transition amplitudes after these expansions are provided in Eqs. (A1) and (A2) of the Appendix for the first- and second-order transition amplitudes, respectively. These expressions explicitly show the dependence on the radial transition amplitudes $U_\kappa(pJ)$ and $U^{(\kappa_n)}_\kappa(p_1J_1, p_2J_2)$, which contain the radial integrals of the electronic wave functions and the photon-electron interaction operator for a given (pair of) multipoles.

Out of the one- and two-photon ionization transition amplitudes, it is straightforward to construct and calculate the ionization rate $dW/d\Omega$ for the biharmonic ionization of atoms

$$\frac{dW}{d\Omega} = \frac{1}{[J_i]} \sum_{M_i M_f m_e} \left| K^{(\omega)} M^{(\omega)}_{M_i M_f m_e} + K^{(2\omega)} M^{(2\omega)}_{M_i M_f m_e} \right|^2, \quad (11)$$

where $[J_i] = (2J_i+1)$ and the prefactors for one- and two-photon ionization are given by $K^{(2\omega)} = \sqrt{\frac{2\alpha\pi^2 F^{(2\omega)}}{\omega}}$ and $K^{(\omega)} = \frac{(2\pi)^{3/2}\alpha F^{(\omega)}}{\omega}$, respectively, and can be derived from the scattering matrix of the S matrix; see, e.g., Ref. [33]. The transition rate $\frac{dW}{d\Omega}$ is used to characterize the ionization process, since the cross section cannot be conveniently defined for a biharmonic ionization process. This general expression of the transition rate contains all relativistic effects as well as all multipoles of the electron-photon interaction. However, in many cases, the nonrelativistic description within the electric dipole approximation is not only fully sufficient, but can be analyzed analytically and provide valuable physical insights.

B. Nonrelativistic limit of biharmonic ionization of *s* electrons

In order to analyze the dependence of the biharmonic rate (11) on the physical parameters such as the beam polarization, photon flux, or the relative phase of the two beam components, we derived a simplified analytical expression. For example, we take the quantization $\hat{z}$ axis along the biharmonic beam propagation direction $\hat{\boldsymbol{k}}$ and restrict the electron-photon interaction to the electric-dipole approximation by taking $J=1$ and $p=1$ in (9). Furthermore, although the transition rate (11) applies generally for the ionization of any atomic shell, in this work, we will present calculations of biharmonic ionization of s electrons only. Finally, for many atoms and ions, the nonrelativistic description of the atomic structure is fully sufficient [34,35] and enables one to analytically investigate the properties of the biharmonic ionization. In the nonrelativistic limit, the radial transition amplitudes are approximately equal to the (strong) transitions between the fine-structure levels. Moreover, these radial integrals also take approximately the same values as their nonrelativistic equivalents, where the electron wave functions are the solutions of the Schrödinger equation. This allows us to reduce the description of electron transitions from five relativistic amplitudes $U_\kappa(pJ)$ and $U^{(\kappa_n)}_\kappa(p_1J_1, p_2J_2)$ to only two transition amplitudes which depend on the orbital angular momentum, $U_l(pJ)$ and $U^{(l_n)}_l(p_1J_1, p_2J_2)$, and sum over all allowed values of the total angular momenta j. In this simplified nonrelativistic picture, only three possible angular momentum ionization pathways remain. The electron can proceed via the one-photon ionization transition $s \to p$, represented by $U_p(E1)$ and the associated phase δ_p, or via two-photon ionization pathways $s \to p \to s$ and $s \to p \to d$, represented by $U^{(p)}_s(E1,E1)$ and $U^{(p)}_d(E1,E1)$ with partial wave phases δ_s and δ_d, respectively. For clarity, the spectroscopic notation for the orbital angular momentum l was employed in the nonrelativistic notation for the radial amplitudes $U_l(pJ)$. This approach allows us to analytically analyze the dependence of the ionization rate on the degree of linear and circular polarization of the fundamental and second harmonic beams, which are given by $P^{(n\omega)}_l = \frac{(\gamma^{(n\omega)})^2-1}{(\gamma^{(n\omega)})^2+1}$ and $P^{(n\omega)}_c = \frac{2\gamma^{(n\omega)}}{(\gamma^{(n\omega)})^2+1}$, respectively.

Considering the above-mentioned simplifications, it is possible to obtain the transition rate for the biharmonic ionization of s electrons in the nonrelativistic limit. Moreover, to analyze the individual contributions to the final photoelectron angular distributions, we split the rate into three parts. The first term $\frac{dW_{\rm sym}}{d\Omega}$ describes the symmetric part of the distribution, which is independent of the sign of the ellipticities of the ω as well as 2ω beams and is always positive. The dichroic contribution to the ionization rate $\frac{dW_{\rm dich}}{d\Omega}$ arises from the interference between different ionization pathways. The individual terms of the dichroic contribution depend on the sign of either of the beam helicities $\gamma^{(2\omega)}$ or $\gamma^{(\omega)}$ (via $P_c^{(n\omega)}$). The last contribution $\frac{dW_{\rm asym}}{d\Omega}$ arises from the interference between one- and two-photon ionization pathways. It remains constant upon reversal of the helicities of *both* beams and exhibits a sign change upon rotation in the polarization plane by $\pi/2$ radians. The ionization rate contributions are given by

$$\begin{aligned}\frac{dW_{\rm sym}}{d\Omega} &= \frac{9\pi\alpha(F^{(\omega)})^2\mu^2}{2\omega F_0}\{|U_p|^2\sin^2\theta\big[1+P_l^{(2\omega)}\cos(2\phi)\big]\}\\ &+\frac{36(F^{(\omega)})^2\pi^2\alpha^2}{\omega^2}\Bigg\{\big|U_s^{(p)}\big|^2\big(P_l^{(\omega)}\big)^2+\big|U_d^{(p)}\big|^2\Bigg[\big(P_l^{(\omega)}\big)^2-3P_l^{(\omega)}\sin^2\theta\big(P_l^{(\omega)}+\cos(2\phi)\big)\\ &+\frac{9}{4}\sin^4\theta\big(1+P_l^{(\omega)}\cos(2\phi)\big)^2\Bigg]+2{\rm Re}\Bigg[U_s^{(p)}U_d^{(p)*}e^{i(\delta_s-\delta_d)}P_l^{(\omega)}\Bigg(P_l^{(\omega)}-\frac{3}{2}\sin^2\theta\big[P_l^{(\omega)}+\cos(2\phi)\big]\Bigg)\Bigg]\Bigg\},\end{aligned} \tag{12}$$

$$\begin{aligned}\frac{dW_{\rm dich}}{d\Omega} &= \frac{108(F^{(\omega)})^2\pi^2\alpha^2}{\omega^2}{\rm Re}\big[iU_s^{(p)}U_d^{(p)*}e^{i(\delta_s-\delta_d)}P_c^{(\omega)}P_l^{(\omega)}\sin^2\theta\sin(2\phi)\big]\\ &-\frac{18(\pi\alpha)^{3/2}(F^{(\omega)})^2\mu}{\sqrt{1+(\gamma^{(2\omega)})^2}\omega^{3/2}F_0^{1/2}}\{2{\rm Re}\big[U_pU_s^{(p)*}e^{i(\delta_p-\delta_s)}e^{i\Phi}P_l^{(\omega)}\gamma^{(2\omega)}\sin(\theta)\sin\phi\big]+{\rm Re}\big[U_pU_d^{(p)*}e^{i(\delta_p-\delta_d)}e^{i\Phi}\\ &\times\big(2P_l^{(\omega)}\gamma^{(2\omega)}\sin\theta\sin\phi+3\sin^3\theta\big[P_c^{(\omega)}\cos\phi\sin(2\phi)-\gamma^{(2\omega)}\sin\phi\big(P_l^{(\omega)}-\cos(2\phi)\big)\big]\big)\big]\},\end{aligned} \tag{13}$$

$$\begin{aligned}\frac{dW_{\rm asym}}{d\Omega} &= \frac{-18(\pi\alpha)^{3/2}(F^{(\omega)})^2\mu}{\sqrt{1+(\gamma^{(2\omega)})^2}\omega^{3/2}F_0^{1/2}}\{2{\rm Re}\big[-iU_pU_s^{(p)*}e^{i(\delta_p-\delta_s)}e^{i\Phi}P_l^{(\omega)}\sin\theta\cos\phi\big]+{\rm Re}\big[iU_pU_d^{(p)*}e^{i(\delta_p-\delta_d)}e^{i\Phi}\\ &\times\big(-2P_l^{(\omega)}\sin\theta\cos\phi+3\sin^3\theta\big[\gamma^{(2\omega)}P_c^{(\omega)}\sin\phi\sin(2\phi)+\cos\phi\big(P_l^{(\omega)}+\cos(2\phi)\big)\big]\big)\big]\},\end{aligned} \tag{14}$$

where $\mu=\sqrt{F^{(2\omega)}F_0}/F^{(\omega)}$ expresses the relative flux between the two beam components with F_0 being the relativistic unit of flux and where the notation $U_l=U_l(E1)$ and $U_l^{(l_n)}=U_l^{(l_n)}(E1E1)$ was used for the sake of brevity. The sum of the symmetric, asymmetric, and dichroic contributions gives the rate of biharmonic ionization

$$\frac{dW}{d\Omega}=\frac{dW_{\rm sym}}{d\Omega}+\frac{dW_{\rm dich}}{d\Omega}+\frac{dW_{\rm asym}}{d\Omega}. \tag{15}$$

The ionization rate for biharmonic ionization of s electrons (15) readily reveals the origin of the elliptical dichroism and describes the contributions of one- and two-photon ionization to the dichroism. The various contributions to the distributions are graphically represented in Fig. 2. The first row depicts the symmetric contribution given by Eq. (12), which is independent of the sign of the beam ellipticities $\gamma^{(\omega)}$ and $\gamma^{(2\omega)}$. The second row emphasizes the different contributions to the dichroism due to the one- and two-photon ionization of atoms. These contributions to the angular distribution of photoelectrons or the angle-differential ionization rate are constructive (green) and destructive (red). The two plots in the second row correspond to two distinct dichroic terms of Eq. (13). The first term arises from the interference of the two two-photon ionization pathways ($s\to p\to s$ and $s\to p\to d$). It possesses a twofold rotational symmetry in the polarization plane and is graphically represented by the right figure of the second line of Fig. 2. The second dichroic term arises from the interference of the one- and two-photon ionization pathways and exhibits one-fold rotational symmetry. It is shown on the left side of the second line of Fig. 2. The positive and negative values of the dichroic contributions swap upon a reversal of the handedness of the biharmonic beam. From the two plots, it becomes clear that these two dichroic contributions may add up, resulting in stronger dichroism than arises from two-photon ionization alone (upper semiplane in Fig. 2), or counteract each other (lower semiplane). The third row of Fig. 2 shows the up-down asymmetry which arises from the interference between the one- and two-photon ionization pathways and is analytically described by Eq. (14). This contribution is invariant upon the simultaneous reversal of the handedness of both beams. The last row shows an example of the photoelectron angular distribution of biharmonic ionization which is given by the sum of all above-listed contributions and corresponds to Eq. (15).

III. RESULTS

To analyze the dichroic properties of the photoelectron angular distributions properly, we define two elliptical dichroism parameters $\Delta_{||}$ and $\Delta_\times$ in accordance with Fig. 1. In general, a dichroism parameter can be defined as

$$\Delta=\frac{W(\gamma^{(\omega)},\gamma^{(2\omega)})-W(-\gamma^{(\omega)},-\gamma^{(2\omega)})}{W(\gamma^{(\omega)},\gamma^{(2\omega)})+W(-\gamma^{(\omega)},-\gamma^{(2\omega)})}, \tag{16}$$

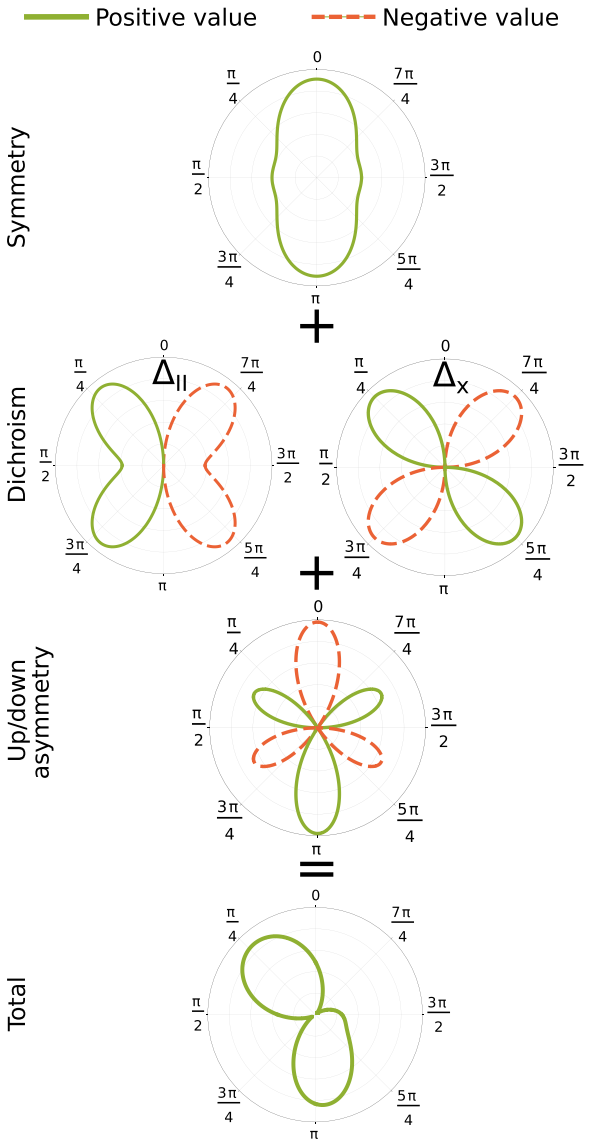

FIG. 2. The angle-differential biharmonic ionization rate (15) can split into symmetric, dichroic, and asymmetric contributions, from top to bottom corresponding to Eqs. (12)–(14), respectively. Contributions arising from interference between different ionization pathways can be either constructive (or positive, full green) and destructive (or negative, dashed red), while the symmetric and final distributions are always positive-valued. The dichroic contribution can be further split into two fundamentally different parts, one with one-fold rotational symmetry within the polarization plane (second line, left) and one with two-fold rotational symmetry (second line, right). The asymmetric term is shown in the third line. The total distribution (fourth row) results from the sum of all the above contributions.

where, for clarity, we explicitly include the dependence on the respective ellipticities and handedness of the two beam components via $\pm\gamma^{(n\omega)}$ and where

$$W(\gamma^{(\omega)},\gamma^{(2\omega)}) = \int_{\phi_1}^{\phi_2} d\phi\, \frac{dW}{d\Omega}(\gamma^{(\omega)},\gamma^{(2\omega)}), \qquad (17)$$

with the integrand given by Eq. (15). The dichroism parameters $\Delta_{||}$ and $\Delta_{\times}$ are defined in the polarization plane, i.e., for $\theta = \pi/2$. More precisely, the parameter $\Delta_{||}$ is then given by Eq. (16) with the integration of the ionization rate carried out in the left half of the angular distribution, $\phi_1 = 0$ and $\phi_2 = \pi$. On the other hand, $\Delta_{\times}$ is obtained from the integral of the ionization rate from $\phi_1 = 0$ to $\phi_2 = \pi/2$ in Eq. (16) *plus* the integral from $\phi_1 = \pi$ to $\phi_2 = 3\pi/2$. This distinction of two dichroism parameters is visualized in Fig. 1 and it is both convenient and necessary in order to effectively disentangle the two distinct contributions to the elliptical dichroism. Explicitly, due to the partial cancellation in the angular integral, the parameter $\Delta_{\times}$ arises from the two-photon ionization process and expresses only the contributions of the first term of Eq. (13), i.e., the right plot in the second line of Fig. 2. The parameter $\Delta_{||}$ arises from the interference between one- and two-photon ionization processes and evaluates only the contributions of the second term of Eq. (13), i.e., the left plot in the second line of Fig. 2.

In the following discussion of these dichroism parameters, we will concentrate on the specific example of the biharmonic ionization of neutral helium atoms in their ground state and for the fundamental photon energy lower than the one-photon ionization threshold. Due to its routine use in experiments at free-electron laser facilities [36,37] and its consideration in previous theoretical treatments of bichromatic ionization [30,38], helium is a reasonable choice for our considerations. However, we expect that our main findings extend to other atomic targets as well. In addition to the target, we will fix the ellipticities of both beam components to $|\gamma^{(\omega)}| = |\gamma^{(2\omega)}| = 0.42$. For these values, the results presented below are most pronounced; however, they are also present if phase and ellipticities are altered.

The total ionization cross section for pure two-photon ionization (relative flux $\mu = 0$) of helium is shown in Fig. 3 (top panel) as a function of photon energy ω. Here, a $1s$ electron is raised to the continuum via a (virtual) intermediate state and the resonant enhancement of the total cross section due to the $1s^2 \to 1s2p$ and $1s^2 \to 1s3p$ transitions can be seen at $\omega = 21.2$ and $\omega = 23.1$ eV. In the lower two panels on the left of Fig. 3, we show the elliptical dichroism parameters defined above for a fixed relative phase $\Phi = \pi/2$ of the two beam components. As was discussed in detail in Ref. [30], the dichroism in pure two-photon ionization can always be maximized by tuning the photon energy such that the intermediate state lies between two such resonances. This fact can be observed in the orange dashed curves in the figure, which were computed from the theory outlined in Sec. II with the second harmonic beam turned off. Since the parameter $\Delta_{||}$ always vanishes in this case, the elliptical dichroism can be fully characterized using the parameter $\Delta_{\times}$, which exhibits the mentioned maximum and minimum to the right of the $1s2p$ resonance. In between the extrema, $\Delta_{\times}$ flips its sign due to a zero crossing of the transition amplitude $U_d^{(p)}$ in the dichroic part of the transition rate (13), around which $l \to l-1$ transitions are favored, contrary to the well-known propensity rules [30,39]. A similar dependence of the dichroism on the photon energy can also be seen around the $1s3p$ resonance.

In the pure two-photon ionization ($\mu = 0$), this dichroic behavior arises from the single term in the first line of the

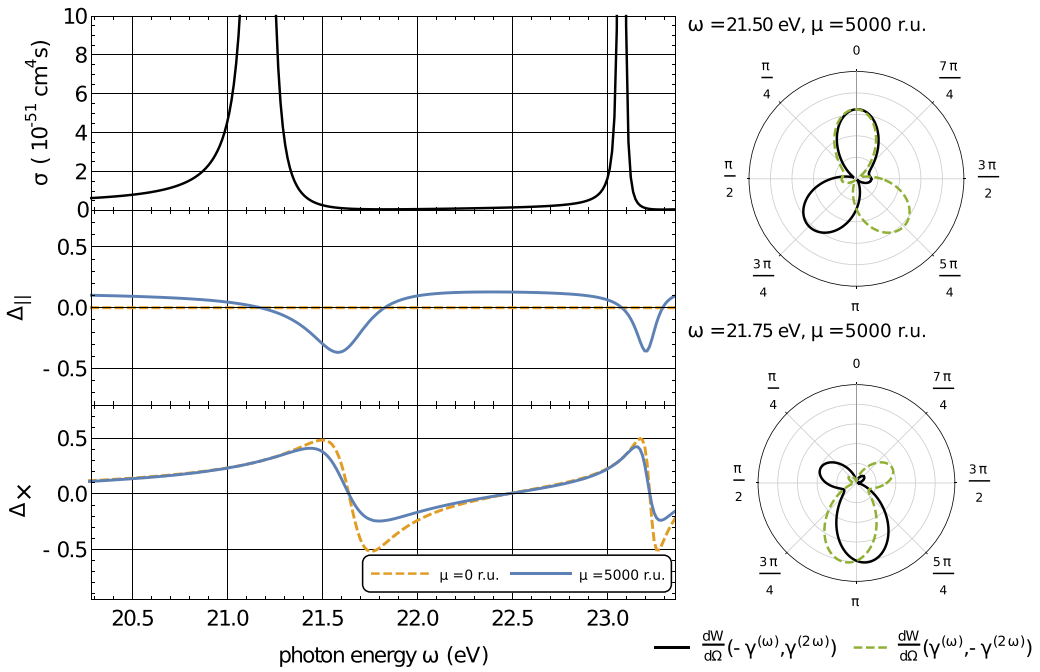

FIG. 3. Dependence of the elliptical dichroism on the fundamental photon energy ω. Left: Total photoionization cross section as function of ω (top). The middle and bottom panels show the elliptical dichroism parameters $\Delta_{||}$ and $\Delta_\times$ as functions of ω and for two values of the relative flux $\mu = \frac{\sqrt{F(2\omega)F_0}}{F(\omega)}$ of the two counter-rotating beam components. Right: Photoelectron angular distributions for relative flux $\mu = 5000$. and two different photon energies. All results were computed for biharmonic ionization of helium with counter-rotating beam components and the following parameters: ellipticities $|\gamma^{(\omega)}| = |\gamma^{(2\omega)}| = 0.42$, intensity $I = 10^{14}$ W/cm^2 of the fundamental beam, and relative phase $\Phi = \pi/2$ between the beam components.

transition rate (13) or, in other words, only from the dichroic contribution shown on the right in the second row in Fig. 2. Let us now turn to the biharmonic ionization, where we will focus on the case of two counter-rotating beam components. If the second-harmonic beam is turned on ($\mu \neq 0$), further contributions shown in Fig. 2 become relevant. In particular, the asymmetric contributions due to the interference of one- and two-photon ionization pathways alter the symmetries of the photoelectron angular distributions. As a consequence, the distributions computed for the biharmonic ionization now possess an up and down asymmetry, shown on the right of Fig. 3. Quantitatively, when compared to the pure two-photon ionization, for the biharmonic ionization the elliptical dichroism parameter $\Delta_\times$ exhibits a similar dependence on the fundamental photon energy (blue curve in the bottom left panel of Fig. 3). Again, close to the $1s2p$ and $1s3p$ resonances, it reaches its extremal values and crosses through zero. This overall behavior is, as before, largely determined by the zero crossing of the amplitude $U_d^{(p)}$ in the transition rates (12)–(14). The angular distributions for which the elliptical dichroism parameter $\Delta_\times$ is maximized are displayed in Fig. 3.

Most importantly for us is the change in dichroic behavior as one goes from pure two-photon ionization to biharmonic ionization. A comparison of the two curves shown in the bottom left panel of Fig. 3 suggests that the elliptical dichroism is *reduced* due to the presence of the second-order harmonic beam. In fact, however, this can be attributed to our choice of dichroism parameters. Indeed, the parameter $\Delta_{||}$ exhibits a markedly different behavior: While it vanishes for all photon energies for $\mu = 0$, it shows a significant amplitude around the resonances for $\mu = 5000$, as shown in the middle left panel in Fig. 3. To demonstrate that the elliptical dichroism in biharmonic ionization is generally significantly *increased*, we define an angle-resolved dichroism parameter introduced, e.g., in Refs. [27,30]. The angle-resolved dichroism is given by $\Delta_\phi(\theta,\phi) = \frac{dW(\gamma^{(\omega)},\gamma^{(2\omega)})/d\Omega - dW(-\gamma^{(\omega)},-\gamma^{(2\omega)})/d\Omega}{dW(\gamma^{(\omega)},\gamma^{(2\omega)})/d\Omega + dW(-\gamma^{(\omega)},-\gamma^{(2\omega)})/d\Omega}$. Within the polarization plane, the dichroism $\Delta_\phi(\theta,\phi)$ will reach a maximum at a certain azimuthal angle(s) $\phi_{\max}$, which generally depends on the beam parameters as well as the chosen target atom. Figure 4 shows the absolute value of the angle-resolved elliptical dichroism $|\Delta_\phi(\theta = \pi/2, \phi_{\max})|$ as a function of the incident beam energy. The dichroism is calculated in the polarization plane at $\phi_{\max}$ for pure two-photon (dashed orange) as well as biharmonic (solid blue) ionization of helium. The figure clearly demonstrates that for most incident photon energies, the angle-resolved dichroism in biharmonic ionization is greater than in pure two-photon ionization. This holds exclusively true for lower incident photon energies; however, it can be broken at near-resonant photon energies due to the dynamic behavior of the transition amplitudes. As the main result of this work, we can therefore conclude that the elliptical dichroism is *enhanced* in the biharmonic ionization when compared to the pure two-photon ionization.

In order to generate an enhanced dichroism signal due to the presence of the second-order harmonic beam, its intensity (or, equivalently, the relative flux μ) needs to be adjusted correctly. In Fig. 5, we display the dichroism parameters $\Delta_\times$ and $\Delta_{||}$ computed as a function of both the fundamental

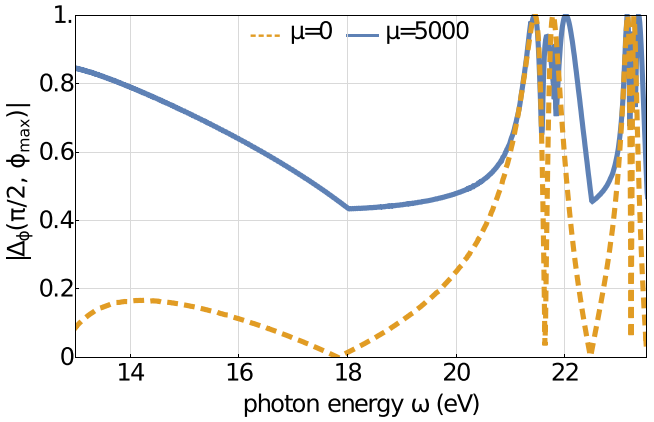

FIG. 4. Angle-resolved elliptical dichroism $\Delta_\phi(\theta = \pi/2, \phi_{\max})$ in two-photon (dashed orange) and biharmonic (solid blue) of helium as a function of incident photon energy.

photon energy ω and the relative flux μ between the two beam components. Here, the relative phase Φ between the beam components was always chosen such that the dichroism parameters are largest for the respective energy ω and relative flux μ. At $\mu = 0$, the dichroism parameter $\Delta_{||} = 0$, while $\Delta_\times$ is at its maximum value. The values of the parameters for nonzero values of μ then strongly depend on the fundamental frequency ω. The ionization becomes dominated by the one-photon ionization process for large values of the relative flux and the dichroism becomes less pronounced. However, practically for all intensities, the elliptical dichroism is present and can be measured in terms of both dichroism parameters. This quite strong dependence on the intensity of the second-order harmonic beam underscores the importance of the coupling of one- and two-photon ionization mechanisms.

The dependence shown in Fig. 3 may serve as an initial guideline for experimental control of the different contributions in Fig. 2 and therefore the elliptical dichroism. While the intensity of the second-order harmonic beam component already leads to a significant modification, the phase between the two beam components offers an additional degree of freedom that allows a rotation of the dichroic contributions within the polarization plane in Fig. 2. A proper theoretical analysis of this influence lies beyond the scope of this work and provides a natural starting point for future investigations.

IV. SUMMARY

In this work, we theoretically investigated the elliptical dichroism in the ionization of atoms by an elliptically polarized biharmonic laser field composed of a fundamental frequency and its second-order harmonic. We treated the process using second-order perturbation theory and independent particle approximation. An extension of this formalism is planned in the frame of the full many-electron open-source atomic code JAC [40]. Here, we derived a simplified expression of the biharmonic ionization rate within the nonrelativistic limit and demonstrated how the shape of the angular distributions arises from the interference of different contributions of one- and two-photon ionization.

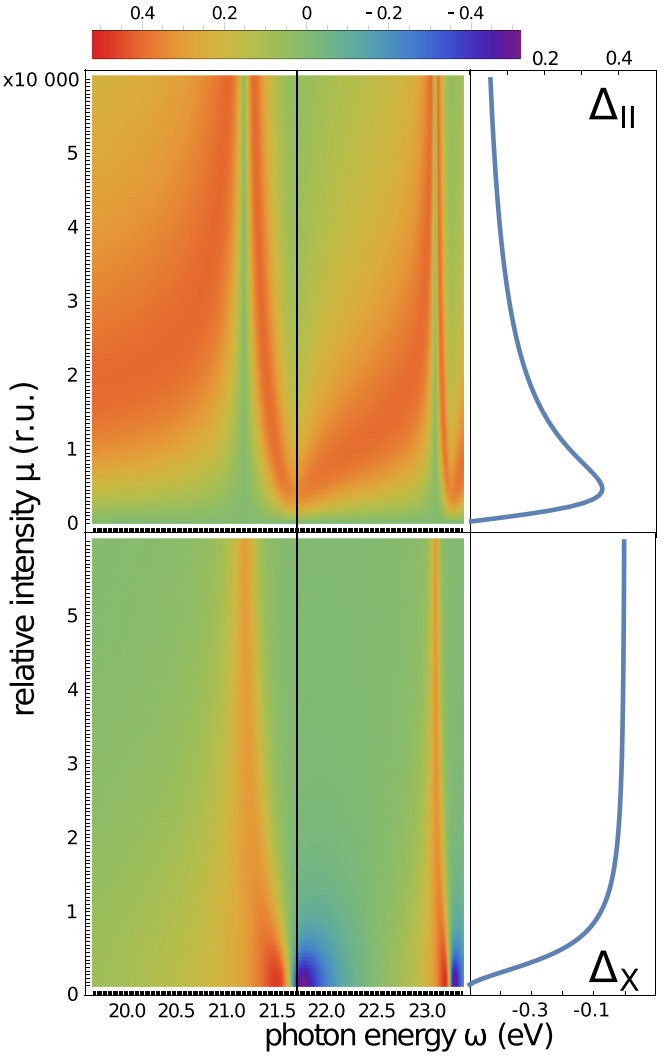

FIG. 5. Elliptical dichroism parameters $\Delta_\times$ (top) and $\Delta_{||}$ (bottom) as a function of the beam fundamental frequency ω and relative flux between the two beam components $\mu = \frac{\sqrt{F^{(2\omega)}F_0}}{F^{(\omega)}}$. The presented dichroism was calculated for biharmonic ionization of helium with the phase difference between the beams Φ, which leads to the largest elliptical dichroism. The blue curves on the right show specifically the μ dependence of the elliptical dichroism at fundamental frequency $\omega = 21.75$ eV. All other parameters are the same as in Fig. 3.

Detailed computations have been carried out for the specific case of the ionization of neutral helium. We found that, in addition to the dependence of the angular distribution on the handedness of the elliptically polarized beam in pure two-photon ionization, such dichroism is also present in the biharmonic ionization. Most importantly, we showed that the dichroism can be enhanced by tuning the intensity of the second-order harmonic beam and the relative phase between the beams properly.

In the $\omega + 2\omega$ ionization, the interference between the two ionization processes only contributes to the photoelectron angular distribution, while it also affects the total ionization yield in the $\omega + 3\omega$ ionization. Although the generation of $\omega + 3\omega$ at XUV energies remains a challenge, it will be

possible in the near future and hence deserves theoretical attention. We hope that the present work will stimulate both theoretical and experimental efforts to investigate this interesting physical process.

ACKNOWLEDGMENTS

The authors greatly appreciate the discussions with Markus Ilchen and Kevin Prince, which provided valuable feedback on the state of current experimental facilities and the beam control possibilities. A.V.V. acknowledges financial support by the Government of the Russian Federation through the ITMO Fellowship and Professorship Program.

APPENDIX: EXPLICIT FORM OF TRANSITION AMPLITUDES

Using the multipole (9) as well as the electron partial wave expansion (10) and carrying out the angular integration over the spatial direction $\hat{\boldsymbol{r}}$ of the electron wave functions, the transition amplitudes (7) and (8) can be written in the following forms:

$$M^{(2\omega)}_{M_i M_f m_e} = 4\pi \sum_{jm_j} \sum_{lm_l} (-i)^l e^{i\delta_\kappa} \langle lm_l, 1/2 m_e | jm_j\rangle Y_{lm_l}(\hat{\boldsymbol{p}}_e) \sum_{JMp} i^{J-p} \big[\hat{\boldsymbol{\epsilon}}^{(2\omega)} \cdot \boldsymbol{Y}^{(p)}_{JM}\big] \times \sum_{m_a} \langle jm_j, JM | j_a m_a\rangle [j]^{-1/2} (-1)^{j_a - m_a} \langle j_a - m_a, J_i M_i | J_f M_f\rangle \langle j \| T_J \| j_a\rangle U_\kappa(pJ) \tag{A1}$$

and

$$\begin{aligned} M^{(\omega)}_{M_i M_f m_e} = {} & 16\pi^2 \sum_{jm_j} \sum_{lm_l} (-i)^l e^{i\delta_\kappa} \langle lm_l, 1/2 m_e | jm_j\rangle Y_{lm_l}(\hat{\boldsymbol{p}}_e) \sum_{J_1 M_1 p_1} \sum_{J_2 M_2 p_2} \sum_{j_n l_n m_n} i^{J_1 - p_1 + J_2 - p_2} \big[\hat{\boldsymbol{\epsilon}}^{(\omega)} \cdot \boldsymbol{Y}^{(p_1)}_{J_1 M_1}\big] \\ & \times \big[\hat{\boldsymbol{\epsilon}}^{(\omega)} \cdot \boldsymbol{Y}^{(p_2)}_{J_2 M_2}\big] [j_n, j]^{-1/2} \langle jm_j, J_2 M_2 | j_n m_n\rangle \sum_{m_a} \langle j_n m_n, J_1 M_1 | j_a m_a\rangle \langle j_a - m_a, J_i M_i | J_f M_f\rangle \\ & \times (-1)^{j_a - m_a} \langle j \| T_{J_2} \| j_n\rangle \langle j_n \| T_{J_1} \| j_a\rangle U^{(\kappa_n)}_\kappa(p_1 J_1 p_2 J_2), \end{aligned} \tag{A2}$$

in terms of radial transition amplitudes for one-photon

$$U_\kappa(pJ) = R_{\kappa\kappa_a}(pJ) \tag{A3}$$

and two-photon ionization

$$U^{(\kappa_n)}_\kappa(p_1 J_1, p_2 J_2) = \sum\!\!\!\!\!\!\int_n \frac{R_{\kappa\kappa_n}(p_2 J_2) R_{\kappa_n \kappa_a}(p_1 J_1)}{\epsilon_{n_a \kappa_a} + \omega - \epsilon_{n_n \kappa_n}}. \tag{A4}$$

The transition amplitudes $U_\kappa(pJ)$ and $U^{(\kappa_n)}_\kappa(p_1 J_1, p_2 J_2)$, of course, depend on the principal quantum numbers of each involved electronic state; however, this dependence was left out from the notation for practical purposes. The angular integration of the space coordinate is given by

$$\langle j_f \| T_J \| j_i\rangle = (-1)^{j_i + j_f - J + 1} [j_i]^{1/2} \langle j_i 1/2, J0 | j_f 1/2\rangle \Pi_{l_i, l, J}, \tag{A5}$$

where $\Pi_{l_i, l, J} = 1$ if $l_i + l + J$ is even and $\Pi_{l_i, l, J} = 0$ otherwise. In the transverse (velocity) gauge, the radial integrals are explicitly given for the magnetic ($p = 0$, or $pJ = MJ$) transitions

$$R_{\kappa_f \kappa_i}(MJ) = i \sqrt{\frac{[J](J+1)}{4J\pi}} \int_0^\infty dr \frac{\kappa_i + \kappa_f}{J+1} j_J(kr) \times [P_i(r) Q_f(r) + Q_i(r) P_f(r)], \tag{A6}$$

where $j_J(x)$ are the spherical Bessel functions, and the radial wave functions $P(r)$ and $Q(r)$ are the large and small components of the radial Dirac wave functions for the orbital with principal and Dirac quantum numbers n_i and κ_i, respectively. These components are obtained from single-electron Dirac equation, with a screening potential in the Hamiltonian, which partially accounts for the interelectronic interaction. We compared a number of different potential models. The core-Hartree potential, which reproduces the binding energies in good agreement with the experimental values, was used to produce the results presented in this work. For the electric transitions ($p = 1$, or $pJ = EJ$)

$$\begin{aligned} R_{\kappa_f \kappa_i}(EJ) = {} & i \sqrt{\frac{[J](J+1)}{4J\pi}} \int_0^\infty dr \Bigg\{ -\frac{\kappa_i - \kappa_f}{J+1} \Bigg[j'_J(kr) \\ & + \frac{j_J(kr)}{kr} \Bigg] [P_i(r) Q_f(r) + Q_i(r) P_f(r)] \\ & + J \frac{j_J(kr)}{kr} [P_i(r) Q_f(r) - Q_i(r) P_f(r)] \Bigg\}. \end{aligned} \tag{A7}$$

In the length gauge, this integral is given by

$$\begin{aligned} R_{\kappa_f \kappa_i}(EJ) = {} & i \sqrt{\frac{[J](J+1)}{4J\pi}} \int_0^\infty dr\, j_J(kr) [P_i(r) P_f(r) \\ & + Q_i(r) Q_f(r)] + j_{J+1}(kr) \Bigg\{ \frac{\kappa_i - \kappa_f}{J+1} \\ & \times [P_i(r) Q_f(r) Q_i(r) P_f(r)] + [P_i(r) Q_f(r) \\ & - Q_i(r) P_f(r)] \Bigg\}. \end{aligned} \tag{A8}$$

The presented results were calculated in the velocity gauge; however, the calculations were performed in both velocity and length gauges to check the consistency and accuracy of our calculations.

[1] C. A. Mancuso, D. D. Hickstein, P. Grychtol, R. Knut, O. Kfir, X.-M. Tong, F. Dollar, D. Zusin, M. Gopalakrishnan, C. Gentry *et al.*, Phys. Rev. A **91**, 031402(R) (2015).

[2] D. B. Milošević and W. Becker, Phys. Rev. A **93**, 063418 (2016).

[3] C. A. Mancuso, D. D. Hickstein, K. M. Dorney, J. L. Ellis, E. Hasović, R. Knut, P. Grychtol, C. Gentry, M. Gopalakrishnan, D. Zusin *et al.*, Phys. Rev. A **93**, 053406 (2016).

[4] S. Odžak, E. Hasović, W. Becker, and D. B. Milošević, J. Mod. Opt **64**, 971 (2017).

[5] A. Gazibegović-Busuladžić, W. Becker, and D. B. Milošević, Opt. Express **26**, 12684 (2018).

[6] J. L. Chaloupka, J. Phys. B **53**, 185601 (2020).

[7] D. Pengel, S. Kerbstadt, D. Johannmeyer, L. Englert, T. Bayer, and M. Wollenhaupt, Phys. Rev. Lett. **118**, 053003 (2017).

[8] S. Kerbstadt, K. Eickhoff, T. Bayer, and M. Wollenhaupt, Adv. Phys. **4**, 1672583 (2019).

[9] G. S. J. Armstrong, D. D. A. Clarke, J. Benda, J. Wragg, A. C. Brown, and H. W. Van Der Hart, Phys. Rev. A **100**, 063416 (2019).

[10] D. B. Milošević, W. Becker, and R. Kopold, Phys. Rev. A **61**, 063403 (2000).

[11] W. Paufler, B. Böning, and S. Fritzsche, Phys. Rev. A **98**, 011401(R) (2018).

[12] S. Skruszewicz, J. Tiggesbäumker, K.-H. Meiwes-Broer, M. Arbeiter, T. Fennel, and D. Bauer, Phys. Rev. Lett. **115**, 043001 (2015).

[13] K. C. Prince, E. Allaria, C. Callegari, R. Cucini, G. De Ninno, S. Di Mitri, B. Diviacco, E. Ferrari, P. Finetti, D. Gauthier *et al.*, Nat. Photon. **10**, 176 (2016).

[14] L. Giannessi, E. Allaria, K. C. Prince, C. Callegari, G. Sansone, K. Ueda, T. Morishita, C. N. Liu, A. N. Grum-Grzhimailo, E. V. Gryzlova *et al.*, Sci. Rep. **8**, 7774 (2018).

[15] M. Di Fraia, O. Plekan, C. Callegari, K. C. Prince, L. Giannessi, E. Allaria, L. Badano, G. De Ninno, M. Trovò, B. Diviacco *et al.*, Phys. Rev. Lett. **123**, 213904 (2019).

[16] E. Allaria, D. Castronovo, P. Cinquegrana, P. Craievich, M. Dal Forno, M. B. Danailov, G. D'Auria, A. Demi-dovich, G. De Ninno, S. Di Mitri *et al.*, Nat. Photon. **7**, 913 (2013).

[17] A. A. Lutman, J. P. MacArthur, M. Ilchen, A. O. Lindahl, J. Buck, R. N. Coffee, G. L. Dakovski, L. Dammann, Y. Ding, H. A. Dürr *et al.*, Nat. Photon. **10**, 468 (2016).

[18] A. N. Grum-Grzhimailo, E. V. Gryzlova, E. I. Staroselskaya, J. Venzke, and K. Bartschat, Phys. Rev. A **91**, 063418 (2015).

[19] N. Douguet, A. N. Grum-Grzhimailo, E. V. Gryzlova, E. I. Staroselskaya, J. Venzke, and K. Bartschat, Phys. Rev. A **93**, 033402 (2016).

[20] E. V. Gryzlova, M. M. Popova, A. N. Grum-Grzhimailo, E. I. Staroselskaya, N. Douguet, and K. Bartschat, Phys. Rev. A **100**, 063417 (2019).

[21] J. Venzke, A. Jaroń-Becker, and A. Becker, J. Phys. B **53**, 085602 (2020).

[22] A. V. Volotka, J. Hofbrucker, and S. Fritzsche (unpublished).

[23] M. Bashkansky, P. H. Bucksbaum, and D. W. Schumacher, Phys. Rev. Lett. **60**, 2458 (1988).

[24] A. Kassaee, M. L. Rustgi, and S. A. T. Long, Phys. Rev. A **37**, 999 (1988).

[25] P. Lambropoulos and X. Tang, Phys. Rev. Lett. **61**, 2506 (1988).

[26] H. G. Muller, G. Petite, and P. Agostini, Phys. Rev. Lett. **61**, 2507 (1988).

[27] N. L. Manakov, A. Maquet, S. I. Marmo, V. Veniard, and G. Ferrante, J. Phys. B **32**, 3747 (1999).

[28] Z.-M. Wang and D. S. Elliott, Phys. Rev. Lett. **84**, 3795 (2000).

[29] S. P. Goreslavski, G. G. Paulus, S. V. Popruzhenko, and N. I. Shvetsov-Shilovski, Phys. Rev. Lett. **93**, 233002 (2004).

[30] J. Hofbrucker, A. V. Volotka, and S. Fritzsche, Phys. Rev. Lett. **121**, 053401 (2018).

[31] N. Douguet, E. V. Gryzlova, E. I. Staroselskaya, K. Bartschat, and A. N. Grum-Grzhimailo, Eur. Phys. J. D **71**, 105 (2017).

[32] E. V. Gryzlova, A. N. Grum-Grzhimailo, E. I. Staroselskaya, N. Douguet, and K. Bartschat, Phys. Rev. A **97**, 013420 (2018).

[33] A. I. Achiezer and V. B. Berestecky, *Quantum Electrodynamics* (Nauka, Moscow, 1969).

[34] J. Hofbrucker, A. V. Volotka, and S. Fritzsche, Phys. Rev. A **94**, 063412 (2016).

[35] J. Hofbrucker, A. V. Volotka, and S. Fritzsche, Phys. Rev. A **96**, 013409 (2017).

[36] M. Meyer, D. Cubaynes, D. Glijer, J. Dardis, P. Hayden, P. Hough, V. Richardson, E. T. Kennedy, J. T. Costello, P. Radcliffe *et al.*, Phys. Rev. Lett. **101**, 193002 (2008).

[37] M. Ilchen, N. Douguet, T. Mazza, A. J. Rafipoor, C. Callegari, P. Finetti, O. Plekan, K. C. Prince, A. Demidovich, C. Grazioli *et al.*, Phys. Rev. Lett. **118**, 013002 (2017).

[38] A. K. Kazansky, A. V. Grigorieva, and N. M. Kabachnik, Phys. Rev. Lett. **107**, 253002 (2011).

[39] U. Fano, Phys. Rev. A **32**, 617 (1985).

[40] S. Fritzsche, Comput. Phys. Commun. **240**, 1 (2019).